Frequency-Wavenumber Processing of Laser-Excited Guided Waves for Imaging Structural Features and Defects

E. B. FLYNN, J.-R. LEE, G. J. JARMER and G. PARK

ABSTRACT

Recent research efforts have demonstrated the ability to remotely and non-destructively excite broadband, multi-mode guided waves in structures through thermoelasticity using a relatively low-powered Q-switched laser. The excited waves can be sensed either locally using one or more transducers or remotely using a laser Doppler vibrometer. Incorporating high-speed mirrors, such a system has been used to effectively and rapidly scan large areas with surface normals as high as 45 degrees at a spatial resolution as small as 0.5 millimeters.

The time and space sampling capability of the laser-excited guided wave system enables the processing of measured signals in the full, three-dimensional Fourier domain: horizontal and vertical in-plane wavenumber and frequency. Operating in the frequency-wavenumber domain, we describe and demonstrate an approach to identify, extract the dispersion curves of, and selectively isolate individual guided wave modes. With the ability to separate individual wave modes, the direction-, frequency-, and mode-dependent wave propagation and scattering behavior can be measured and utilized for imaging defects.

We introduce two imaging algorithms for utilizing mode-separate measurements. The first, which we show to be effective for area-spanning defects, makes direct estimates of the mode- and frequency-dependent wavelength at each imaging point in the structure. The second, which is more effective for identifying small defects, images the energy of backscattered waves present at each point. We demonstrate the frequency-wavenumber processing and imaging procedures on three example structures: an aluminum plate with a hole, a steel pipe with wall-thinning, and a complex composite component with a local delamination.

Eric B. Flynn, Los Alamos National Laboratory, MS T-001, Los Alamos, NM 87545, United States

INTRODUCTION

Structural Health Monitoring

Automated embedded monitoring systems, traditionally referred to as structural health monitoring (SHM) systems, while ideal, have so far had limited success in living up to their initial promise. Such systems suffer from an information problem. Discrete arrays of transducers, even relatively dense ones, do not provide enough information to separate abnormal from natural structural behavior. While comparing live measurements against reference (presumably "healthy") measurements, or baselining, can lead to an indication of damage, it usually provides little characterizing information about the damage and has primarily only been proven effective in environment-stable settings.

Among SHM technologies, the implementation of ultrasonic guided waves (UGW) has received much attention and shown to be the most effective for detecting small-scale defects [1]. This is because the use of actively-induced, high-frequency, wide-band elastic waves comes closest to solving the information problem. However, baselining, which again has had only limited success in the field, is still required on all but the most simple of structures.

With the ability to virtualize an array of sensors with sub-wavelength spacing, non-contact scanning systems can provide significantly more information than embedded sensors are able to offer. Modern technologies include air-coupled roving transducers [2], scanning laser Doppler vibrometers [3], and scanning laser-generated ultrasound (SLGU) [4].

Scanning laser-generated ultrasound (SLGU)

An SLGU system involves a scanning pulsed or Q-switched laser that generates a non-destructive ultrasonic wave in a structure through local thermoelastic expansion. The generated wave is in turn sensed by a fixed-point laser-Doppler vibrometer or a permanently bonded sensor. Generating waves at a fine grid of inspection points allows one to rapidly reconstruct full wave fields which can qualitatively show the interaction of waves with structural defects such as cracks, corrosion, or delamination that are otherwise not visible to the human eye. Figure 1 shows a simplified diagram of an SLGU system. SLGU systems use a scanning laser for excitation only, so they do not rely on the measurement of scattered light. This provides three significant benefits:

- Range is limited by the focus of the laser beam (tens of meters), rather than the intensity of the scattered light (meters) or acoustic coupling (centimeters).
- Near-zero degree angle of incidence on the structure is not required. This allows SLGU systems to scan complicated structures as well as scan large/multiple regions from a fixed instrument position.
- Surface preparation of the scanning area is usually not necessary.

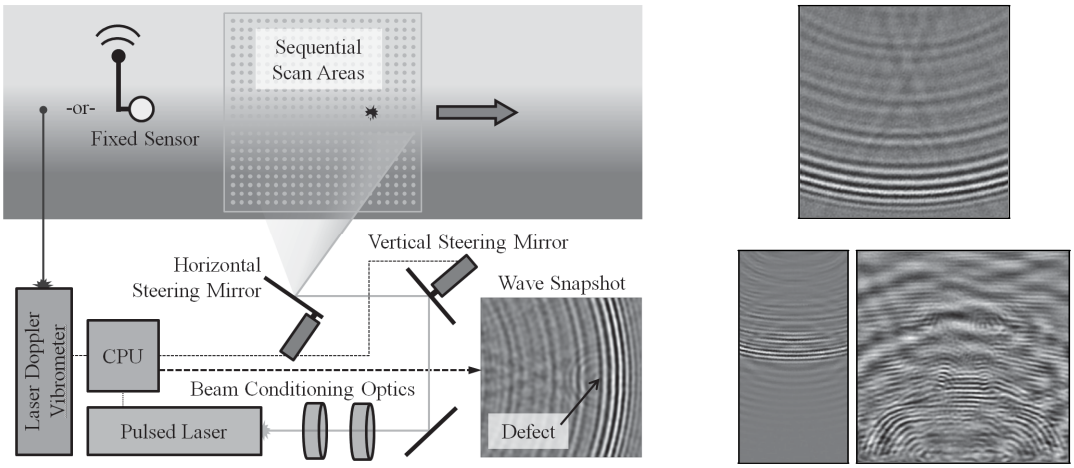

Figure 1. Conceptual diagram of an SLGU System. Wave snapshots for plate (upper right), pipe (lower right) and wing section (lower far right) test structures.

PRELIMINARIES

The 3D Data Matrix

The system scans over a uniform, two-dimensional, N by M grid of points on the structure, exciting each grid point with a single laser pulse and recording T time samples of the response with a single fixed-position piezoelectric transducer. A full scan then generates a three-dimensional N by M by T matrix, indexed by x-direction, y-direction, and time samples, respectively, along each dimension. Assuming reciprocity holds, this matrix could be thought of as either the response at the transducer due to excitation at each grid point, or the response at each grid point due to an excitation by the transducer. The former is the true representation, while the latter, a spatial time history (or animation) of the response due to a single point-source excitation, serves as a more intuitive interpretation. The wave snapshots of the three test structures shown in Figure 1 are the renderings of single slices in time of the three-dimensional data matrices.

Frequency-Wavenumber Processing

The Fourier transform along all three dimensions of the time-space matrix results in a frequency-wavenumber matrix. The Fourier transform can also be applied along a subset of the dimensions to form a mix-domain matrix, such as a frequency-space matrix. Filtering can be applied independently in the wavenumber and frequency domains. Further, band-pass filtering over a range of angles in the 2D wavenumber space allows one to selectively pass only waves propagating in a particular direction. For more details on frequency-wavenumber filtering for guided waves, see [5]. Throughout this work, we performed filtering using a Fourier-domain Blackman-Harris window with cutoffs defined as the half-power points.

Notation

x, y, t	x-direction and y-direction coordinate and time

k_x, k_y, f	x-direction and y-direction wavenumber and temporal frequency
θ	Direction angle relative to positive x-direction
$m \in \{A_0, S_0\}$	Lamb wave mode

We will attempt to represent filters and transformations applied to the full 3D space-time matrix, $\boldsymbol{V}$, in a consistent way. A triple of superscripts (e.g. (0A1)) will indicated the domain transformation for the x, y, and time dimensions, respectively. Tokens "0", "1", and "A" will indicate the time/spatial domain, the frequency/wavenumber domain, and the analytical signal along that direction. Quadruple subscripts will indicate the filter ranges in terms of Lamb Wave modes, wave propagation direction, wavenumber, and frequency. A "~" token indicates no filtering in that direction or domain. Here are a couple of examples:

$V^{(000)}_{(A_0,\sim,\sim,[f_c \pm B_f])}(x,y,t)$: Space-time domain signal filtered to the A0 mode and the temporal frequency band $f_c \pm B_f$

$V^{(0A1)}_{(\sim,[45°,135°],[k_c \pm B_k],\sim)}(x,y,f)$: Space-frequency signal that is analytic along y direction, direction filtered from 45 to 135 degrees, and bandpass filtered in the wavenumber domain.

TEST STRUCTURES

We tested the proposed imaging algorithms on three test structures:

- A 3 mm aluminum plate with a 2 mm hole
- A 20 mm thick steel pipe with internal ellipsoid-shaped, 8 cm by 13 cm, 40% wall thinning
- A 2.2 mm composite wing section with a 2 cm impact delamination

Diagrams of these structures, including the position of the imaging regions, sensing transducers, and defects, are provided in Figure 2. Scans were performed on the opposite surfaces from those displayed in the figure. The images for the pipe section were effectively "unrolled" through interpolation so that Cartesian coordinates were mapped on to the curved surface.

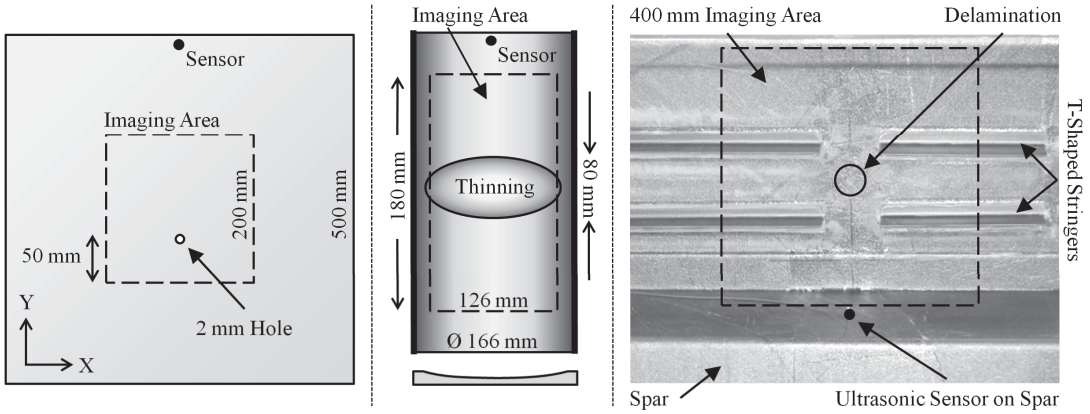

Figure 2. Test structures (from left to right): Plate, pipe, composite wing. Scans were performed on the opposite surfaces of the structures.

WAVE MODE FILTERING

Frequency-Wavenumber Curve Estimate

For a given plate material and thickness, each Lamb wave mode has a one-to-one relationship between frequency and Wavenumber, forming a frequency-wavenumber curve. For a reasonably uniform plate, the majority of the energy will fall into the wavenumber-frequency bins that are along theses lines. The ratio of frequency to the wavenumber is equal to the wave phase velocity at that point on the curve, and the slope df/dk is equal to the wave group velocity. Estimating these curves enables one to selectively filter individual modes and identify their velocities. We estimate the frequency-wavenumber curves in the following manner:

1. Calculate the magnitude of the frequency-wavenumber spectrum and slice along the primary wave propagation direction (e.g. 90° or $k_x = 0$).
2. Find the bin with the max value and assign that as the first curve point:

$$\left\{\hat{k}_y\left(f_0, m\right), f_0\right\} = \arg\max_{k_y, f} \left|V_{(\sim)}^{(111)}\left(0, k_y, f\right)\right|. \quad (1)$$

3. Move one frequency bin the right and find the max within a specified wavenumber range. Repeat until last frequency bin:

$$\hat{k}_y\left(f_n, m\right) = \arg\max_{k_y \in \left[\hat{k}_y\left(f_{n-1}, m\right) \pm B_k\right]} \left|V_{(\sim)}^{(111)}\left(0, k_y, f_n\right)\right|. \quad (2)$$

4. Repeat 3, except moving to the left from the first curve point (f_{-1}).
5. Fit the identified points to low-order curve function
6. Remove the mode through filtering (see below) and repeat from 2

For a non-uniform plate, the extracted curves represent estimates of the *average* frequency-wavenumber curves over the imaging area.

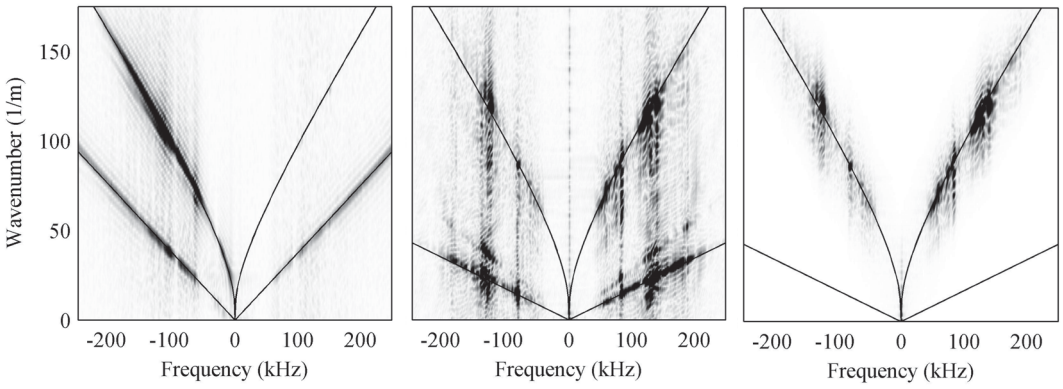

Figure 3. Frequency-wavenumber magnitude plots with S_0 (lower) and A_0 (upper) curve estimates. Plate unfiltered (left), wing unfiltered (middle,) and wing filtered to A_0 mode (right).

Mode Filtering

Mode filtering is performed by applying a frequency-dependent, band-pass filter in the wavenumber domain about the estimated frequency-wavenumber curve. Figure 3 shows the estimated S_0 and A_0 frequency-wavenumber curves and the frequency-wavenumber magnitude plots along 90° before and after filtering about the A_0 mode.

IMAGING APPROACHES

Estimated Mode Wavelength Imaging (EMWI)

In this imaging approach, we attempt to estimate the wavelength of the propagating waves at each spatial sample point of the structure for a given Lamb wave mode and frequency. This is done by first transforming the mode-filtered matrix to the space-frequency domain, taking a single frequency slice, and calculating the analytic signal along the dominant propagating direction (in our case, along the Y-direction). The resulting 2D spatial matrix is then band-pass filtered about a series of central wavenumbers, k_c, and the magnitude (envelope) for each result is calculated. The inverse of the central wavenumber that maximizes the magnitude for each spatial sample point is used as the wavelength estimate for that point. This can be succinctly described by:

$$\hat{\lambda}(x,y,f,m) = \left(\arg\max_{k_c} \sum_{t} \left| V^{(0\mathrm{A}1)}_{(m,\sim,[k_c \pm B_k],\sim)}(x,y,f) \right| \right)^{-1}. \tag{3}$$

In practice, we found that the estimate is improved by averaging the wavelength estimate across multiple, closely space, frequency slices.

Figure 4 shows the estimation results for three test structures. The estimator parameters used were as follows:

$$\begin{aligned} &\text{Plate:} && m = \mathrm{A}_0, && f_s = 100 \text{ kHz}, && B_k = 0.05 \\ &\text{Pipe} : && m = \mathrm{S}_0, && f_s = 100 \text{ kHz}, && B_k = 0.06 \\ &\text{Wing:} && m = \mathrm{A}_0, && f_s = 50 \text{ kHz}, && B_k = 0.04 \end{aligned} \tag{4}$$

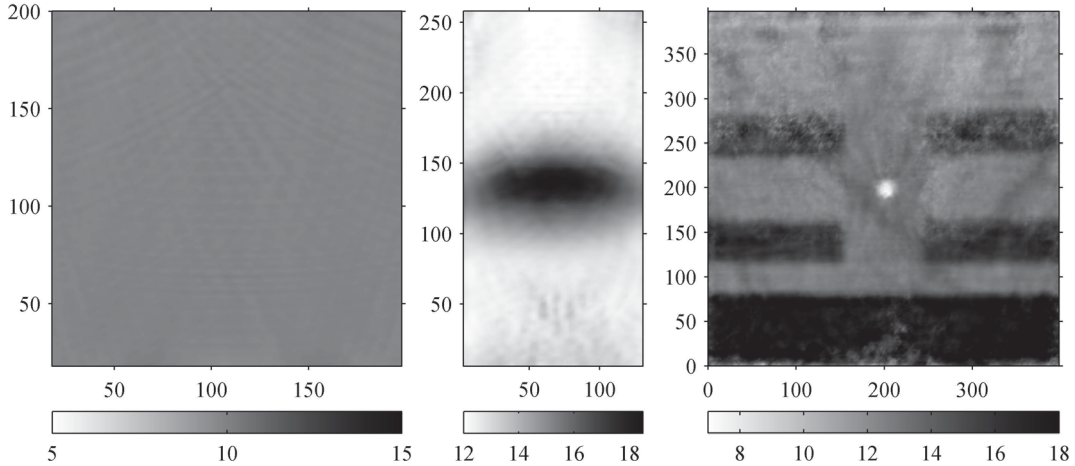

Figure 4. Maps of S_0 and A_0 wavelength estimates (in mm) for flat plate, pipe, and composite wing test structures, respectively. Axis units also in mm.

The uniformity of the aluminum plate is evident in the estimation map while the location of the hole is not. The ellipse-shaped wall-thinning in the pipe is clearly identifiable by an increase in the wavelength of the S_0 mode from approximately 13 mm to 18 mm. In the composite-wing estimation map, the delamination is indicated by a decrease in the wavelength of the A_0 mode from 12 mm to 7 mm. Also identifiable are the four stringers, the spar, and, more subtlety, two diagonal composite laminate overlap regions.

Wave Scatter Imaging (WSI)

While we found wavelength estimation to be an effective and quantitative means of defect identification, its application is limited to area-spanning defects and not appropriate for defects such as out-of-plane cracks and small holes. For these types of defects, we are instead interested in capturing the wave scattering behavior of the potential defect.

We achieve this by filtering the data matrix to a single wave mode and in the direction opposite the initial propagation direction (i.e. back towards the transducer). The magnitude of the frequency-band-passed, time-analytic signal (envelope) is then mapped to each spatial sample point by gating the signal to the time of flight from the transducer to that point, for that mode and center frequency. This is done for several frequency bands and the images are summed:

$$I(x,y,m,\theta) = \sum_{f} \left| V^{(00\mathrm{A})}_{(m,[\theta \pm B_\theta],\sim,[f \pm B_f])}\left(x,y,\tau\left(x,y,m,f\right)+\Delta t\right)\right|^2 \tag{5}$$

where $\tau(x,y,m,f)$ is the time of flight of Lamb wave mode m at center frequency f from the imaging point (x,y) to the sensing transducer. This frequency-dependent time of flight is determined using the group velocity approximated from the slope of the estimated frequency-wavenumber curves. This approach effectively follows the wave as it moves across the structure, but only images the energy that is moving in the opposite direction of the primary wave (scatter) as it passes each point. The parameter Δt causes the algorithm to figuratively "peek ahead" to when the wave scatter is more developed, improving SNR at the cost of localization.

Figure 5 shows the resulting images for the three test structures. The intensity at each imaging point was normalized by the total sensed energy following laser excitation at that point. The following parameters were used:

$$\begin{aligned}
&\text{Plate:} \quad m = \mathrm{A}_0,\ \theta = 90°,\ B_\theta = 60°\ \ \Delta t = 20\ \mu\mathrm{s} \\
&\text{Pipe:} \quad m = \mathrm{S}_0,\ \theta = 90°,\ B_\theta = 60°\ \ \Delta t = 50\ \mu\mathrm{s} \\
&\text{Wing:} \quad m = \mathrm{A}_0,\ \theta = 90°,\ B_\theta = 60°\ \ \Delta t = 40\ \mu\mathrm{s}
\end{aligned} \tag{6}$$

The intensity of the imaged scatter in the case of the plate and pipe was easily separable from the background noise intensity. In the pipe, however, S_0 backscatter was only present at the leading edge of the ellipse-shaped wall thinning. For the composite wing section, while the A_0 backscatter from the delamination is visible, its intensity is masked by the normal backscatter from the other geometric features in the structure.

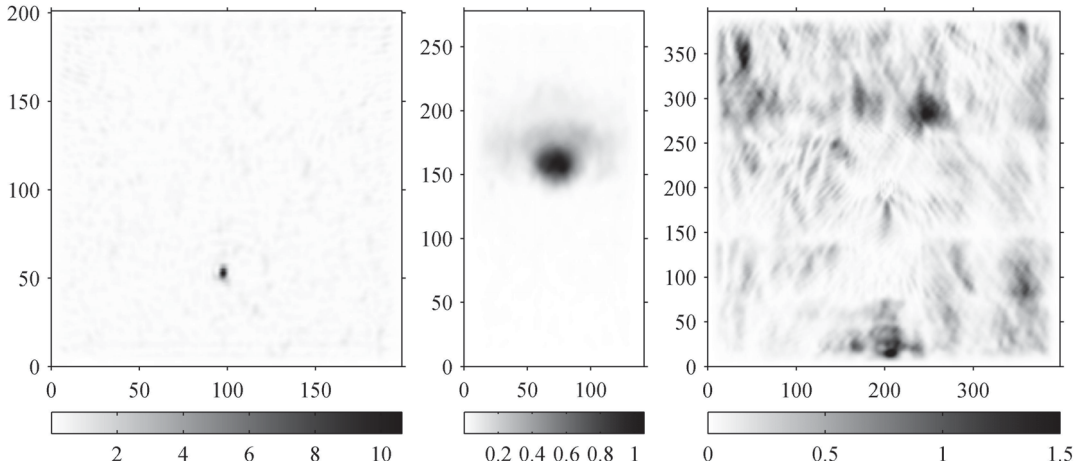

Figure 5. Wave scatter images for flat plate, pipe, and composite wing, respectively. Normalized intensity in p.p.m.. Axis units in mm.

CONCLUSIONS

We presented two imaging approaches made possible through wave-mode filtering of scanning laser-generated ultrasound data. Estimated mode wavelength imaging has the potential to provide detailed, qualitative information for damage identification and characterization, but is limited to area-spanning defects. A next iteration on this approach would be to estimate full frequency-wavelength curves for each spatial sample point and to map these to material properties, such as plate thickness, using theoretical dispersion curves.

Wave scattering imaging, in the basic form we have described, is capable of resolving small defects, but suffers in the presence of other natural scatter sources. We hypothesize that this approach could be improved by capturing the wave mode and wavenumber functional dependency of the scatter intensity. This dependency could aide in characterizing defects and separating them from nature features.

This research was supported by the Laboratory Directed Research and Development program at Los Alamos National Laboratory (UR 12-01506) and the Leading Foreign Research Institute Recruitment Program through the National Research Foundation of Korea funded by the Ministry of Education, Science and Technology (2011-0030065).

REFERENCES

1. Croxford A, Wilcox P, Drinkwater B, Konstantinidis G. Strategies for guided-wave structural health monitoring. Proceedings of the Royal Society A: Mathematical, Physical and Engineering Science. 2007;463(2087):2961.
2. Michaels TE, Michaels JE. Application of Acoustic Wavefield Imaging to Non-Contact Ultrasonic Inspection of Bonded Components. AIP Conference Proceedings. 2006;820(1):1484–1491.
3. Staszewski WJ, Lee BC, Mallet L, Scarpa F. Structural health monitoring using scanning laser vibrometry: I. Lamb wave sensing. Smart Materials and Structures. 2004 Apr 1;13(2):251–260.
4. Lee J-R, Shin H-J, Chia CC, Dhital D, Yoon D-J, Huh Y-H. Long distance laser ultrasonic propagation imaging system for damage visualization. Optics and Lasers in Engineering. 2011 Dec;49(12):1361–1371.
5. Ruzzene M. Frequency–wavenumber domain filtering for improved damage visualization. Smart Materials and Structures. 2007 Dec 1;16(6):2116–2129.